JOURNAL OF GUIDANCE, CONTROL, AND DYNAMICS
Vol. 20, No. 3, May–June 1997

Optimal Steering for North–South Stationkeeping of Geostationary Spacecraft

Jean Albert Kechichian*
The Aerospace Corporation, El Segundo, California 90245

The problem of north–south stationkeeping of geostationary spacecraft using electric thrusters is analyzed. Pure yawing with short-duration low-thrust arcs applied infrequently is assumed, and the dynamics are cast in continuous form to obtain an analytic steering law in the inclination-node (i, Ω) space that brings the spacecraft back to the ideal initial orbit orientation for the initiation of a free-drift period that satisfies the inclination constraint for the longest possible duration. This problem is posed as a minimum-time navigation problem between two i, Ω pairs and is similar to the Zermelo problem of navigating a ship in strong variable currents. The simple linear steering law thus obtained is easy to use and fuel optimal compared to other suboptimal strategies for travel between two given (i, Ω) pairs.

I. Introduction

CONTROL strategies for the north–south stationkeeping of geostationary spacecraft with chemical propulsion have been thoroughly documented in the literature.[1–7] There exists an ideal drift in the inclination-right ascension of the ascending node (i, Ω) space that results in the satisfaction of the inclination deadband constraint for the longest possible duration. This inclination deadband is defined by $0 \leq i \leq i_{\max}$, with $i_{\max}$ the maximum allowable inclination. Once the deadband is consumed, an impulsive maneuver will target to certain optimized initial conditions in i and Ω to continue the satisfaction of the deadband constraint. Considerable fuel can be saved if the low I_{sp} chemical rockets are replaced by high I_{sp} electric engines to effect the same stationkeeping maneuvers, thereby extending the operational life of these satellites. However, these maneuvers cannot be carried out in an essentially instantaneous manner, but must be implemented in small incremental steps spanning several weeks or more, depending on the level of the thrust acceleration and the frequency of the incremental maneuvering. The inherent long duration of these low-thrust maneuvers must be factored in the design of the maneuver strategy inasmuch as it must account for the natural drift that takes place before the completion of the maneuver sequence. This paper adopts, as an example for illustration purposes, the ideal drift cycle in i, Ω as the fundamental cycle to repeat, and casts the dynamics of this problem in a continuous fashion to convert it into a navigation problem of minimum-time travel between given i, Ω pairs, not unlike the well-known Zermelo problem in optimal control theory. The control is now a steering angle that defines the direction of the change in the i, Ω region to be effected by the small incremental ΔV at that particular moment in the overall sequence. It is assumed that these small ΔV are large enough to overcome the natural drift in the opposite direction such that the ideal initial conditions are recovered in time. We begin in Sec. II with the description of the idealized (i, Ω) drift dynamics due to Kamel and Tibbitts,[7] which will be used in the design of the optimal steering strategy shown in the subsequent sections.

Section III shows how the relevant linearized variation of parameters equations are used to calculate the changes in the orbit plane orientation due to small thrust arcs. In Sec. IV, a suboptimal strategy that does not factor the natural drift in i and Ω between successive thrust arcs is depicted. This strategy consists of applying the thrust arc at the current common line of nodes of the current orbit and the final target orbit. The more efficient strategy of Sec. V creates new intermediate target orbits and applies the thrust arc at the common line of nodes of the current orbit and the intermediate target orbit, thereby factoring the natural drift in i, Ω between maneuvers in the transfer design.

II. General Analysis of North–South Drift: Impulsive Maneuvering

The equations of motion governing the evolution of the inclination i and ascending node Ω of a satellite orbit in near-circular condition are given by[7]

$$\dot{i} = -\frac{1}{na^2 s_i}\frac{\partial R}{\partial \Omega} \tag{1}$$

$$\dot{\Omega} = \frac{1}{na^2 s_i}\frac{\partial R}{\partial i} \tag{2}$$

Here s_i is sin i and c_i is cos i; these equations are valid for any value of the semimajor axis a and inclination i but restricted to small eccentricity e. Here n is the orbit mean motion and R the perturbing function due to Earth's triaxiality, the moon, and the sun:

$$\begin{aligned} R = {} & \tfrac{1}{4}\mu n_m^2 a^2\left[\left(1-\tfrac{3}{2}s_i^2\right)\left(1-\tfrac{3}{2}s_{i_m}^2\right)+\tfrac{3}{4}s_{2i}s_{2i_m}c_{\Omega-\Omega_m}\right. \\ & \left.+\tfrac{3}{4}s_i^2 s_{i_m}^2 c_{2(\Omega-\Omega_m)}\right]+\tfrac{1}{4}n_s^2 a^2\left[\left(1-\tfrac{3}{2}s_i^2\right)\left(1-\tfrac{3}{2}s_{i_s}^2\right)\right. \\ & \left.+\tfrac{3}{4}s_{2i}s_{2i_s}c_{\Omega}+\tfrac{3}{4}s_i^2 s_{i_s}^2 c_{2\Omega}\right]+\tfrac{3}{2}n^2 J_2 R_e^2\left(\tfrac{1}{3}-\tfrac{1}{2}s_i^2\right) \end{aligned} \tag{3}$$

where $\mu = 1/82.3$, the ratio of the mass of the moon to the combined masses of the Earth and the moon; $n_m = 0.23$ rad/day, the moon's orbit mean motion; $n_s = 0.017203$ rad/day, the sun's apparent orbit mean motion; i_m the moon's orbit equatorial inclination; i_s the sun's apparent orbit equatorial inclination; Ω_m the right ascension of the ascending node of the moon's orbit with respect to the Earth equator; J_2 the second zonal harmonic of the Earth potential; and R_e the mean equatorial Earth radius. Now the moon's inclination with respect to the ecliptic i_M stays constant at 5.145 deg, but its ascending node Ω_M in degrees varies as a linear function of time according to $\Omega_M = 259.183 - 0.05295t$ with t time in Julian days measured from Jan. 1, 1900, 12 h. The regression rate of 0.05295 deg/day is such that it takes 18.6 years for Ω_M to regress by 360 deg. This regression of the node is due to the solar gravity perturbation on the moon's orbit. The effect of this ecliptic nodal regression is to induce a variation of both the equatorial i_m and Ω_m of the lunar orbit such that $i_s - i_M \leq i_m \leq i_s + i_M$ or $18.3 \leq i_m \leq 28.59$ deg and $-13.0 \leq \Omega_m \leq 13.0$ deg. This can be shown from simple spherical trigonometry, such as that from Fig. 1, and from the law of cosines and the law of sines, respectively,

$$c_{i_m} = c_{i_M}c_{i_s} - s_{i_s}s_{i_M}c_{\Omega_M} \tag{4}$$

$$s_{\Omega_m} = \frac{s_{i_M}s_{\Omega_M}}{s_{i_m}} \tag{5}$$

Received Sept. 3, 1996; revision received Dec. 23, 1996; accepted for publication Jan. 7, 1997.

*Engineering Specialist, Astrodynamics Department. Associate Fellow AIAA.

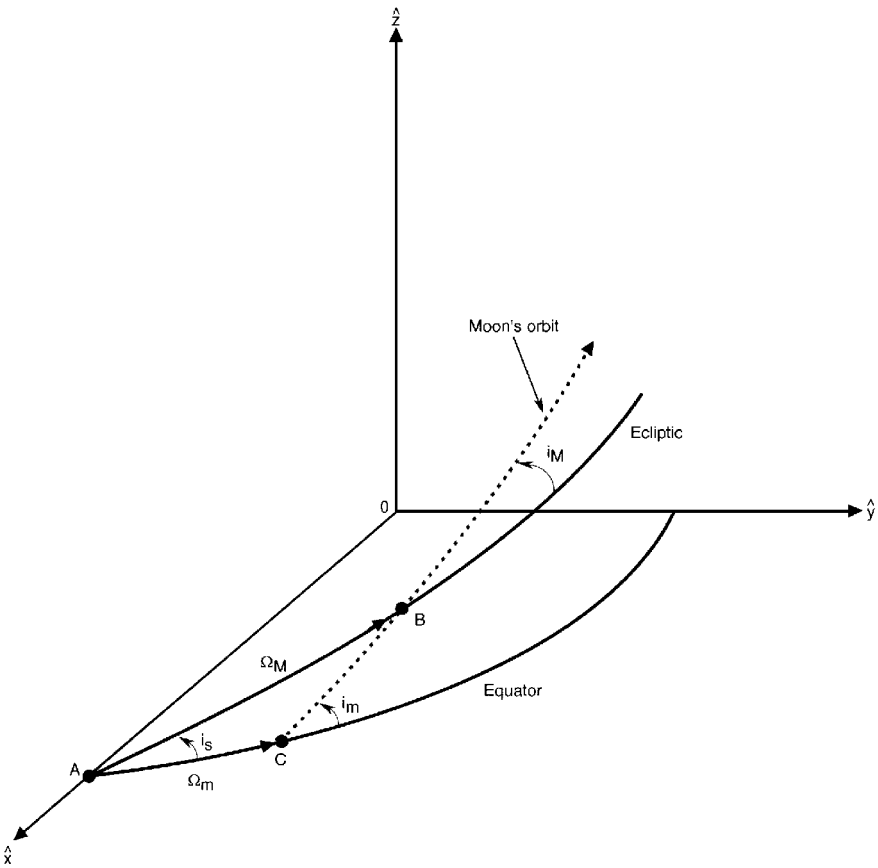

Fig. 1 Sun and moon orbit geometry.

Both i_M and i_s are fixed, but Ω_M varies according to the linear law mentioned such that i_m varies according to Eq. (4) and, finally, Ω_M varies according to Eq. (5). The moon's orbit inclination with respect to the equator and its equatorial ascending node vary with the same period as Ω_M (18.6 years). If the variables i and Ω are changed to $h_1 = s_i s_\Omega$ and $h_2 = s_i c_\Omega$, then Eqs. (1) and (2), which are singular at $i = 0$, will be transformed to the set

$$\dot{h}_1 = \frac{c_i}{na^2}\frac{\partial R}{\partial h_2} \tag{6}$$

$$\dot{h}_2 = \frac{-c_i}{na^2}\frac{\partial R}{\partial h_1} \tag{7}$$

This can be seen from

$$\frac{\partial R}{\partial h_1} = \frac{\partial R}{\partial i}\frac{\partial i}{\partial h_1} + \frac{\partial R}{\partial \Omega}\frac{\partial \Omega}{\partial h_1} \qquad \frac{\partial R}{\partial h_2} = \frac{\partial R}{\partial i}\frac{\partial i}{\partial h_2} + \frac{\partial R}{\partial \Omega}\frac{\partial \Omega}{\partial h_2}$$

and because $s_i = (h_1^2 + h_2^2)^{1/2}$, $\tan\Omega = h_1/h_2$, we have

$$\frac{\partial i}{\partial h_1} = \frac{s_\Omega}{c_i} \qquad \frac{\partial i}{\partial h_2} = \frac{c_\Omega}{c_i} \qquad \frac{\partial \Omega}{\partial h_1} = \frac{c_\Omega}{s_i} \qquad \frac{\partial \Omega}{\partial h_2} = -\frac{s_\Omega}{s_i}$$

such that the preceding two expressions yield $\partial R/\partial i$ and $\partial R/\partial \Omega$ as

$$\frac{\partial R}{\partial i} = c_i\left[s_\Omega\frac{\partial R}{\partial h_1} + c_\Omega\frac{\partial R}{\partial h_2}\right] \tag{8}$$

$$\frac{\partial R}{\partial \Omega} = s_i\left[c_\Omega\frac{\partial R}{\partial h_1} - s_\Omega\frac{\partial R}{\partial h_2}\right] \tag{9}$$

We can now use these expressions in Eqs. (1) and (2) with $\dot{h}_1 = c_i s_\Omega \dot{i} + s_i c_\Omega \dot{\Omega}$ to obtain Eq. (6), and, similarly, with $\dot{h}_2 = c_i c_\Omega \dot{i} - s_i s_\Omega \dot{\Omega}$ to obtain Eq. (7).

For near-equatorial orbits or small i, $c_i \cong 1$ such that the system in Eqs. (6) and (7) can now be cast in the canonical form by way of a quadratic Hamiltonian H in the nonsingular variables h_1 and h_2, after a change of variable from time t to Ω_M (Ref. 7). Kamel and Tibbitts[7] have shown that the differential equations in h_1 and h_2 reduce to a linear system with constant coefficients and, therefore, can be solved in closed form. This simplification amounts to the effective averaging out of the slowly varying fluctuations in h_1 and h_2 with a period of 18.6 years. The equilibrium solution is obtained from $\mathrm{d}h_1/\mathrm{d}\Omega_M = 0$ and $\mathrm{d}h_2/\mathrm{d}\Omega_M = 0$ or, using the subscript e for equilibrium, by $\Omega_e = 0$, $i_e = \sin^{-1}(h_{2e})$. This corresponds to an inertially fixed orbit plane, also called the invariant plane, with its line of nodes along the intersection of the ecliptic and equatorial planes. The inclination i_e is a function of the semimajor axis and for the synchronous altitude $a/R_e = 6.61072$, $i_e = 7.5$ deg (Ref. 7). If our inclination tolerance is larger than 7.5 deg, then the optimal strategy consists of placing the satellite in an orbit inclined at exactly 7.5 deg such that it will never require any north–south stationkeeping maneuver. These maneuvers, however, are necessary if the inclination constraint is less than 7.5 deg. In this case, optimal maneuvering strategies must be devised such that, for example, the constraint is satisfied for the longest time possible between two such maneuvers. Now the motion of the unitized angular momentum vector with components h_1 and h_2, or in other words, the motion of the orbit plane itself described by the Eulerian angles Ω and i, consists of a small oscillation about the equilibrium solution whose period is also a function of the orbit semimajor axis.[7] For the synchronous altitude, it is roughly equal to 54 years. Kamel and Tibbitts[7] have shown that the two first-order differential equations can be reduced to the harmonic oscillator type

$$\frac{\mathrm{d}^2 h_1}{\mathrm{d}\Omega_M^2} + \omega^2 h_1 = 0 \tag{10}$$

with period $P = 2\pi/\omega$. The general solution of the motion is written in terms of equations that describe an anticlockwise ellipse with center at $(0, h_{2e})$ in the (h_1, h_2) domain, with semiminor axis along h_1 and semimajor axis along the h_2 axis. This ellipse represents the precession cycle of the orbital angular momentum about its equilibrium position with a period of roughly 54 years (Ref. 7).

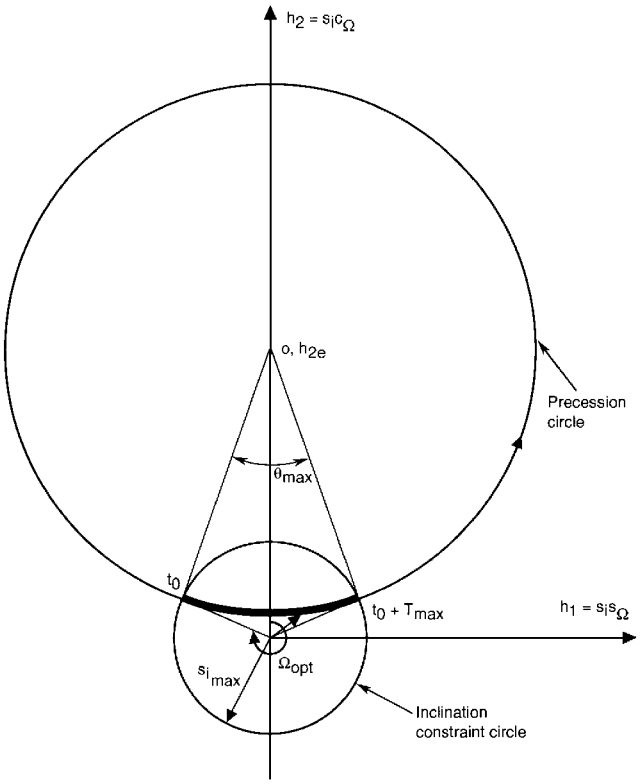

Fig. 2 Optimal drift within inclination constraint circle.[1]

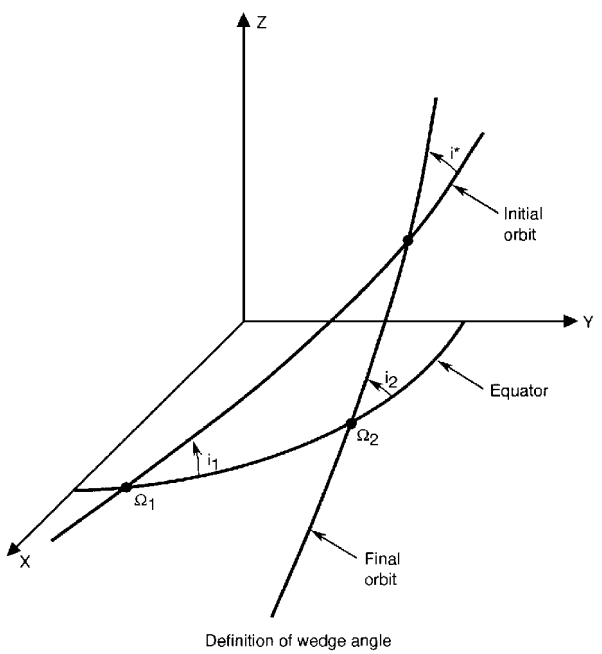

Fig. 3 Wedge angle at relative ascending node.

To the zeroth order, this ellipse is essentially approximated by a circle centered at $(0, h_{2e})$. The polar coordinates (s_i, Ω) are used to represent a point (h_1, h_2) on the precession circle, and if the inclination must remain below a given maximum $i \leq i_{\max}$, then this inclination constraint can be represented by the interior of the circle centered at the origin with radius $s_{i\max}$ (Fig. 2). The precession time taken from an initial point (h_{10}, h_{20}) at $t = t_0$ to a point (h_1, h_2) at time t is proportional to the subtended angle θ, as shown in Fig. 2. Then the linear relationship between θ and $T = (t - t_0)$ is simply given by $T = \theta P/(2\pi)$.

The inclination constraint cannot be satisfied forever, but if the initial values of (Ω_0, i_0) are chosen in an optimal way, then the time between maneuvers can be maximized. Fuel-minimizing strategies can also be devised if higher maneuvering frequencies are tolerated. The former strategy is achieved by choosing $i_0 = i_{\max}$ and $\Omega_0 = 3\pi/2 + \theta_{\max}/2$, with $\theta_{\max} = 2\sin^{-1}(s_{i_0}/h_{2e})$ and with the total elapsed time between t_0 and $t_0 + T$ given by $T_{\max} = \theta_{\max} P/(2\pi)$. The arc between t_0 and $t_0 + T_{\max}$ (Fig. 2) remains for the longest possible time inside the inclination constraint circle, and at time $t_0 + T_{\max}$, an impulsive maneuver must recover the initial node Ω_0 without changing the inclination, which is now the same as i_0. Figure 3 shows the relative geometry of initial and final orbits at maneuver time with nodes Ω_1 (premaneuver) and Ω_2 (postmaneuver), respectively, and identical $i_1 = i_2 = i_{\max}$. The postmaneuver node Ω_2 is, of course, equal to the target value of Ω_0. The post-ΔV orbit will then correspond to the initial orbit that starts the precession cycle until $i_{\max}$ is about to be violated again. The inclination decreases from $i_{\max}$ to a minimum without going through zero, for one-half of the precession time $T_{\max}$, and then it increases to $i_{\max}$ at the end of the cycle with its node at Ω_1. The angle i^* is called the wedge angle, and it represents the inclination of one orbit relative to the other. An impulsive ΔV applied at the intersection of these two orbits rotating the orbit by i^* will, therefore, achieve the condition Ω_2, $i_{\max}$ that starts the precession cycle. From spherical trigonometry, the wedge angle i^* is computed from $c_{i^*} = c_{\Omega_1 - \Omega_2} s_{i_1} s_{i_2} + c_{i_1} c_{i_2}$, and with $i_1 = i_2 = i_{\max}$, $c_{i^*} = c_{\Omega_1 - \Omega_2} s^2_{i_{\max}} + c^2_{i_{\max}}$. The ΔV is obtained from $\Delta V = 2V \sin(i^*/2)$.

III. Mechanics of Low-Thrust Maneuvering

The mechanics of low-thrust inclination control for the case where the orbit is near-circular is analyzed next. The out-of-plane motion is described by the following two equations linearized about a reference circular orbit:

$$\frac{d\Delta i_x}{d\upsilon} = \frac{a_0^2}{\mu_e} c_{\theta'} f_h \qquad \frac{d\Delta i_y}{d\upsilon} = \frac{a_0^2}{\mu_e} s_{\theta'} f_h$$

where Δi_x and Δi_y are the components of the change in the inclination $\Delta \boldsymbol{i}$ along the inertial $\hat{x}$ and $\hat{y}$ directions. The $\hat{x}$, $\hat{y}$ plane is the plane of the initial reference circular orbit of semimajor axis a_0 and mean motion n. The angular position of the spacecraft at time t measured from the $\hat{x}$ axis is given by the angle θ' and the rates are with respect to the nondimensional time $\upsilon = nt$. Here μ_e is the gravity constant of the Earth. The instantaneous acceleration vector $\boldsymbol{f}$ has components f_r, f_θ, and f_h in the rotating Euler–Hill frame, and the thrust vector $\boldsymbol{T}$ is completely defined by the yaw and pitch angles θ_h and θ_t. $\Delta \boldsymbol{i} = \Delta i_x \hat{x} + \Delta i_y \hat{y}$ with $\Delta i_x = \Delta i c_{\theta'}$, $\Delta i_y = \Delta i s_{\theta'}$, and Δi obtained from the variation of parameters equation $di/dt = (r f_h/h) c_\theta$ where θ is now the angular position measured from the ascending node. When the spacecraft is initially on the reference circular orbit, we have $\theta = 0$, $r = a_0$, and $h = n a_0^2$ such that for a small impulse $\Delta \boldsymbol{V}$ applied along the direction $\boldsymbol{\beta} = (\beta_r, \beta_\theta, \beta_h)$ we have $\Delta i = (\Delta V/n a_0)\beta_h$ because $\Delta t f_h = \Delta V \beta_h$. Therefore, $\Delta i_x = (\Delta V/n a_0)\beta_h c_{\theta'}$, $\Delta i_y = (\Delta V/n a_0)\beta_h s_{\theta'}$, and $\Delta \boldsymbol{i} = (\Delta i/n a_0)\beta_h \hat{r}$. The nondimensional rates in terms of f_h, $d\Delta i_x/d\upsilon$, and $d\Delta i_y/d\upsilon$ are now readily obtained. For near-circular orbits, $\theta' \cong nt = \upsilon$ and $c_{\theta'} \cong c_\upsilon$, $s_{\theta'} \cong s_\upsilon$ and with T and m standing for the thrust magnitude and spacecraft mass, respectively, the linearized equations reduce to the form

$$\frac{d\Delta i_x}{d\upsilon} = \frac{k}{a_0 n^2} c_\upsilon s_{\theta_h} \tag{11}$$

$$\frac{d\Delta i_y}{d\upsilon} = \frac{k}{a_0 n^2} s_\upsilon s_{\theta_h} \tag{12}$$

where $k = T/m$. Now if only pure yawing is used, i.e., $\theta_h = \pm\pi/2$, then with $g = k/(a_0 n^2)$ and after a full revolution of continuous thrust with $\theta_h = \pi/2$ for one-half revolution and $\theta_h = -\pi/2$ for the other half, the maximum rotation of the initial orbit plane will be given by

$$\Delta i_{\max} = 4g \tag{13}$$

Because $k = T/m = 2P/(mc)$ with $c = I_{sp} \cdot g_r$ and with P thrust power, c exhaust velocity, I_{sp} specific impulse, and g_r acceleration of gravity, the expression (13) can be reduced to $\Delta i_{\max} = 8P/m I_{sp} g_r a_0 n^2$, and it is given in radians, when P is in watts, m

in kilograms, I_{sp} in seconds, g_r in meters per square second, a_0 in meters, and n in radians per second. The power of the jet is the time rate of expenditure of the kinetic energy of the ejected matter $E_{jet} = \frac{1}{2}\Delta mc^2$ such that $P = \dot{E}_{jet} = \frac{1}{2}\dot{m}c^2 = \frac{1}{2}Tc$. The power transmitted to the vehicle is $P_{veh} = T\dot{V}$, where $\dot{V}$ is the vehicle velocity. Let $a_0 = 42{,}241$ km with corresponding mean motion $n = (\mu_e/a_0^3)^{1/2} = 7.272205 \times 10^{-5}$ rad/s or 360 deg/day for the two-body geostationary orbit. This value of a_0 is chosen for illustrative purposes inasmuch as Earth's inertial rate is actually equal to 360.985 deg/day instead of 360 deg/day used here. Let us suppose that $m = 1134$ kg, and a resistojet with $I_{sp} = 295$ s and jet power of 1 kW such that the vehicle is imparted an acceleration $k = f = T/m = 2P/(mc) = 6.096119 \times 10^{-4}$ m/s^2. A continuous application of this acceleration during one revolution or 24 h will result in a $\Delta V = f \cdot t = 52.670$ m/s with an equivalent Δi_{max} given by $\Delta i_{max} = 0.62544$ deg. If we now consider a 1-h thrust arc spread around the line of nodes of current and target orbits, then the angular travel will be $360/24 = 15$ deg at geosynchronous Earth orbit (GEO). The relative rotation of the orbit plane corresponding to this burn will be obtained from

$$\Delta i_x = \frac{k}{a_0 n^2}\int_{-7.5}^{7.5} c_\upsilon \, d\upsilon = 7.1240179 \times 10^{-4} \text{ rad}$$

and

$$\Delta i_y = \frac{k}{a_0 n^2}\int_{-7.5}^{7.5} s_\upsilon \, d\upsilon = 0$$

such that $\Delta i = (\Delta i_x^2 + \Delta i_y^2)^{1/2} = 0.040817$ deg. For an inclination deadband of 0.3 deg, and letting $i_0 = 0.3$ deg, $h_{2e} = s_{7.5} = 0.130526$, we have $\theta_{max} = 4.5979$ deg, $\Omega_0 = 272.298$ deg, $T_{max} = 251.912$ days with period $P = 54$ years. The change in Ω or $\Delta\Omega = \Omega_{init} - \Omega_{final}$ is obtained from $\Delta\Omega = -2(90 - 2.298) = -2\Omega_1 = -175.404$ deg, which is the same as $\Delta\Omega = \Omega_1 - \Omega_2$. Now the wedge angle is calculated with $i_1 = i_2 = 0.3$ deg and $\Omega_1 - \Omega_2 = -175.404$ deg such that $i^* = 0.5995$ deg. Because 1 h of pure out-of-plane thrusting rotates the orbit by 0.0408 deg, it will take 0.5995 deg/0.0408 deg/h = 14.693 h of total thrust of 1 h each at the line of nodes of current and final orbits. We can thrust either 1 h per revolution at, say, the ascending common node or 2 h per revolution with 1 h each at the ascending and descending common nodes, respectively. The total inclination change can, therefore, be achieved in 14.693 revolutions or days or 7.346 revolutions or days. This requires a total ΔV of 32.246 m/s.

The impulsive ΔV can be computed from $\Delta V/V = 2i_{max}|\sin(\Delta\Omega/2)| = 0.0104635$, with $i_{max} = 0.3$ deg, such that with $V = (\mu_e/a_0)^{1/2}$, $\Delta V = 32.142$ m/s, which is only slightly smaller than the 32.246 m/s for the low-thrust solution. This shows that the 1-h thrust arcs at GEO are effectively as efficient as the impulsive solution with almost no ΔV loss. However, the continuous 24-h acceleration that rotates the orbit by 0.62544 deg requiring 52.670 m/s of total ΔV can be achieved much more efficiently by applying a single impulse requiring a ΔV of $\Delta V = 2V\sin(\delta/2)$, with $\delta = 0.62544$ deg and $V = (\mu_e/a_0)^{1/2} = 3.071902$ km/s such that $\Delta V = 33.532$ m/s for a savings of 19.138 m/s. This shows that it is not economical to thrust continuously for a complete revolution to effect an inclination change. Now the impulsive ΔV to effect the 0.5995-deg inclination change, which is the wedge angle i^*, can also be computed from $\Delta V = 2V\sin(i^*/2) = 32.142$ m/s. If we let $i_{max} = 0.1$ deg for a tighter tolerance, then $\theta_{max} = 1.532304$ deg, $\Omega_0 = 270.766152$ deg, $T_{max} = 83.89$ days, and $\Delta\Omega = -178.467695$ deg requiring an impulse of $\Delta V = 10.731$ m/s. The wedge angle (Fig. 3) is now $i^* = 0.199982$ deg. Because the 1-h low-thrust accelerations produce a relative rotation of the orbit plane of 0.040817 deg, requiring a quasiimpulsive $\Delta V = 2.187$ m/s, the total ΔV of 10.731 m/s for this tighter deadband can be achieved in less than five acceleration cycles requiring three to five revolutions at GEO to achieve. This time frame is still negligible when compared to the drift period of 83 days and, therefore, these low-thrust maneuvers can be accomplished quickly without worrying too much about the drift during the maneuvering period. This will not be the case for lower thrust accelerations. In this case, the orbit rotation to repeat the drift cycle will require a much longer period of time and, therefore, appropriate strategies must be designed to account for the drift accumulated during the longer maneuvering period such that the optimal initial conditions are achieved at the end of the maneuver sequence.

IV. Suboptimal Strategy

Given the initial (i_1, Ω_1) and final (i_2, Ω_2) orbits, an inclination change through an angle i' at their common line of nodes is required. Because of the lower acceleration level of the low-thrust maneuver, a smaller rotation i'' is achieved instead around point B (Fig. 4). The inclination i_j and node Ω_j can be obtained from spherical trigonometry. If we wait in this orbit for some given duration, then i_j and Ω_j will drift to new values at the time of the next thrusting cycle, such that the thrust must now be applied around the new common line of nodes of the present orbit and the target orbit. This suboptimal strategy does not factor the drift in the maneuver design and, therefore, is less efficient in recovering the target conditions. From the triangle ABC and the law of sines and cosines, and with $\Delta\Omega = \Omega_2 - \Omega_1$,

$$s_{AB} = \frac{s_{i_2} s_{\Delta\Omega}}{s_{i'}} \tag{14}$$

$$c_{AB} = \frac{-c_{i_2} + c_{i_1} c_{i'}}{s_{i_1} s_{i'}} \tag{15}$$

From the triangle ABD, we have

$$-c_{i_j} = -c_{i_1} c_{i''} + s_{i_1} s_{i''} c_{AB}$$

and using Eq. (15),

$$c_{i_j} = c_{i_1} c_{i''} - (s_{i''}/s_{i'})\left(c_{i_1} c_{i'} - c_{i_2}\right) \tag{16}$$

This equation determines i_j without ambiguity because $0 \le i_j \le \pi$. In a similar manner, we have

$$s_{\Delta\Omega_j} = \frac{s_{i''} s_{AB}}{s_{i_j}} \tag{17}$$

$$c_{i''} = c_{i_1} c_{i_j} + s_{i_1} s_{i_j} c_{\Delta\Omega_j} \tag{18}$$

Using Eqs. (14) and (17), an expression for $\Delta\Omega_j = \Omega_j - \Omega_1$ is obtained:

$$\tan\Delta\Omega_j = \frac{s_{i_1} s_{i''} s_{AB}}{c_{i''} - c_{i_1} c_{i_j}}$$

or substituting in Eq. (14) yields

$$\tan\Delta\Omega_j = \frac{s_{i_1} s_{i''} s_{i_2} s_{\Delta\Omega}}{s_{i'}\left(c_{i''} - c_{i_1} c_{i_j}\right)} \tag{19}$$

with c_{i_j} given by Eq. (16). Therefore, we can solve for the angles i_j and Ω_j and apply another small low-thrust maneuver at the new line of nodes of this orbit with the unchanged target orbit by replacing Ω_1 by Ω_j and i_1 by i_j and repeating the same calculations until Ω_2, i_2 is finally reached. For our earlier $i_{max} = 0.1$ deg example, we have $i_1 = i_2 = 0.1$ deg, $i' = 0.199982$ deg, $\delta i = i'' = 0.040817$ deg, $i_j = 0.059189$ deg, $\Omega_2 = 270.766152$ deg, $\Omega_1 = 90 - 0.766152 = 89.233848$ deg, $\Delta\Omega = -2(90 - 0.766152) = -178.467695$ deg or, identically, $\Delta\Omega = \Omega_2 - \Omega_1 = 181.532304$ deg, and $\Omega_j = \Omega_1 + \Delta\Omega_j = 88.705515$ deg. Also, $h_1 = s_{i_j} s_{\Omega_j} = 1.032783 \times 10^{-3}$, $h_2 = s_{i_j} c_{\Omega_j} = 2.333766 \times 10^{-5}$, and $h_1(0) = s_{i_1} s_{\Omega_1} = 1.745172 \times 10^{-3}$, $h_2(0) = s_{i_1} c_{\Omega_1} = 2.333761 \times 10^{-5}$, such that $\Delta h_{eq} = \{[h_1 - h_1(0)]^2 + [h_2 - h_2(0)]^2\}^{1/2} = 7.123891 \times 10^{-4}$ represents the change achieved in the h_1, h_2 plane by the 1-h out-of-plane low-thrust maneuver. Similar Δh_{eq} variations will slowly result in achieving the target parameters i_2, Ω_2 for the initiation of the natural drift cycle. In this strategy we can ignore the small drift that takes place between the application of two such subsequent maneuvers because i_j and Ω_j will then drift and, therefore, be updated by orbit determination or analytically, before the next maneuver. Figure 5 shows the angular momentum vector $\boldsymbol{h}$ and its change $\boldsymbol{\delta h}$ due to the low-thrust maneuver, such that $\boldsymbol{h} + \boldsymbol{\delta h}$ is now the postmaneuver angular momentum vector. Because the thrust is

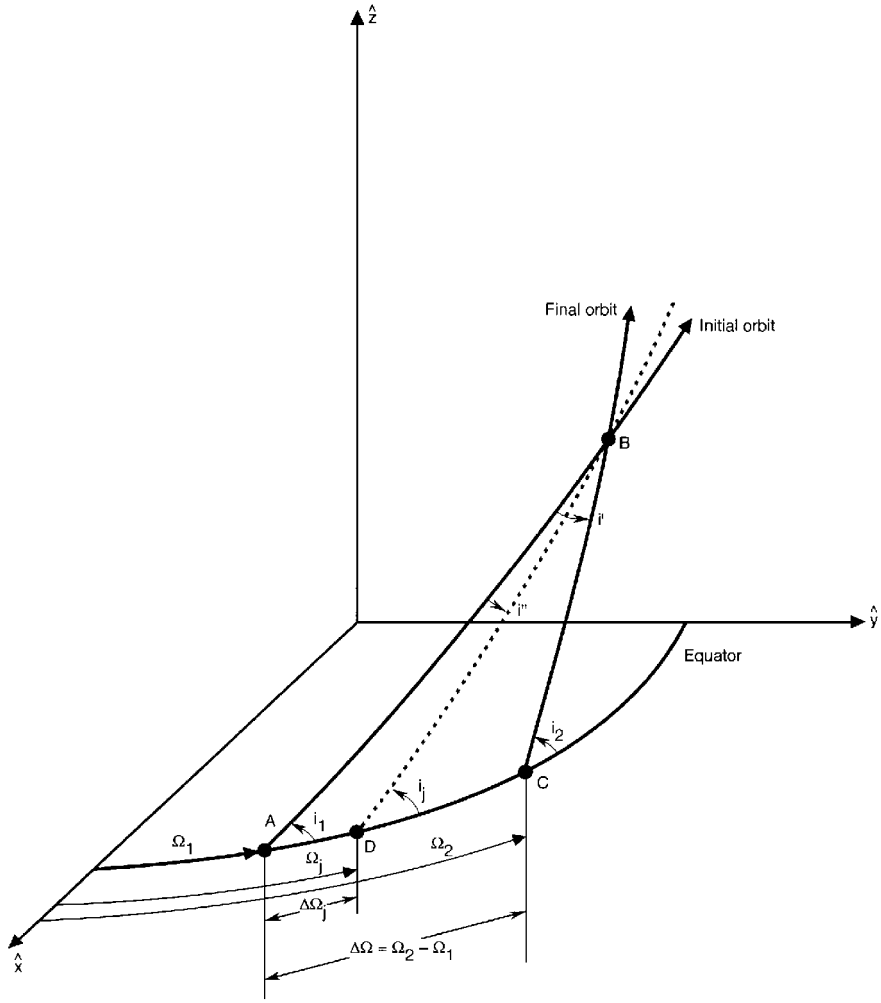

Fig. 4 Orbit plane rotation at relative node.

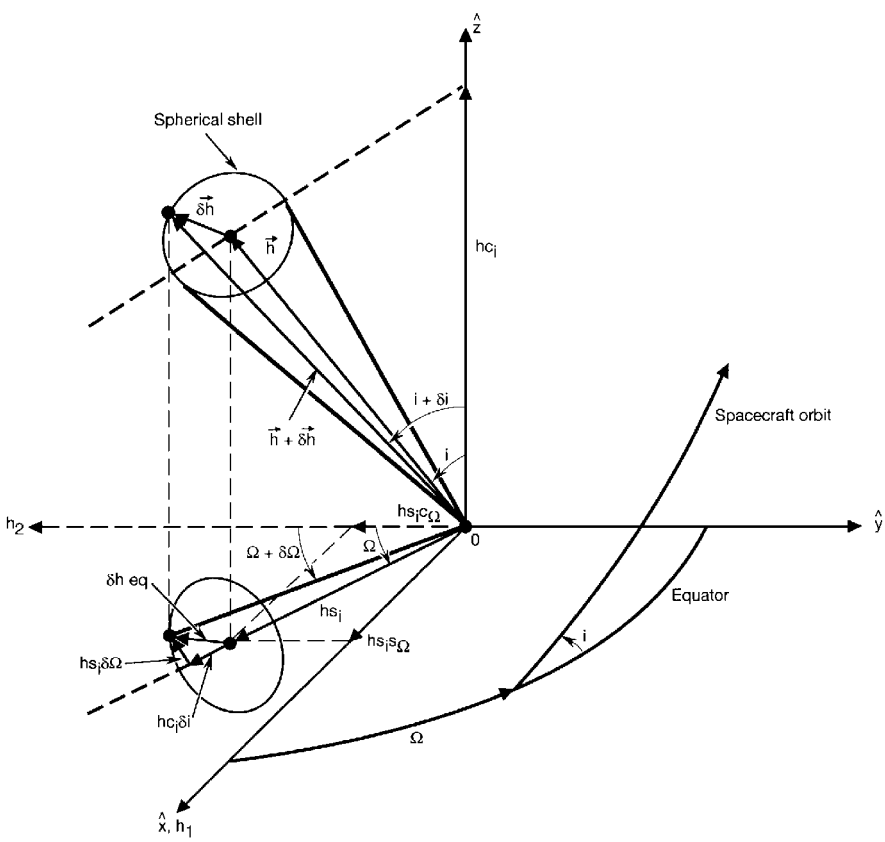

Fig. 5 Capability ellipse due to small thrust arc.

applied normal to the orbit plane, the length of $\boldsymbol{h}$ remains unchanged while its direction is changed. Therefore, a thrust arc of duration Δt will place $\boldsymbol{h}$ along the circular edge of the spherical shell shown in Fig. 5, for all possible locations of this thrust arc along the spacecraft orbit. The projection of $\boldsymbol{h}$ onto the equatorial plane, which defines the $\hat{h}_1$ and $\hat{h}_2$ axes, is hs_i inclined at an angle Ω from the $\hat{h}_2$ axis or the $-\hat{y}$ inertial axis, and the projection of the spherical shell is, in general, an ellipse centered at the tip of the hs_i vector. The angular momentum vector can be written as $\boldsymbol{h} = hs_i s_\Omega \hat{x} - hs_i c_\Omega \hat{y} + hc_i \hat{z}$, and for a small δi rotation, $\boldsymbol{h} + \boldsymbol{\delta h} = hs_{i+\delta i} s_\Omega \hat{x} - hs_{i+\delta i} c_\Omega \hat{y} + hc_{i+\delta i} \hat{z}$, which leads after expansion to $\boldsymbol{\delta h} = hc_i s_\Omega \delta i \hat{x} - hc_i c_\Omega \delta i \hat{y} - hs_i \delta i \hat{z}$ with magnitude $|\boldsymbol{\delta h}| = h\delta i$. The magnitude of the projection of $\boldsymbol{\delta h}$ onto the equatorial plane is given by

$$|\boldsymbol{\delta h}_{\text{eq}}| = \left(h^2 c_i^2 \delta i^2\right)^{\frac{1}{2}} = hc_i \delta i \tag{20}$$

Similarly, for a small $\delta\Omega$ change, the projection of $\boldsymbol{\delta h}$ onto the h_1, h_2 plane has magnitude

$$|\boldsymbol{\delta h}_{\text{eq}}| = hs_i \delta\Omega \tag{21}$$

and for the more general case of a simultaneous δi and $\delta\Omega$ change, $(\boldsymbol{h} + \boldsymbol{\delta h})_{\text{eq}} = hs_{i+\delta i} s_{\Omega+\delta\Omega} \hat{x} - hs_{i+\delta i} c_{\Omega+\delta\Omega} \hat{y}$, leading to

$$|\boldsymbol{\delta h}_{\text{eq}}| = h\left(c_i^2 \delta i^2 + s_i^2 \delta\Omega^2\right)^{\frac{1}{2}} \tag{22}$$

Now from $h_1 = s_i s_\Omega$ and $h_2 = s_i c_\Omega$, we have

$$\delta h_1 = c_i s_\Omega \delta i + s_i c_\Omega \delta\Omega \qquad \delta h_2 = c_i c_\Omega \delta i - s_i s_\Omega \delta\Omega$$

and, therefore,

$$\delta h_{\text{eq}} = \left(\delta h_1^2 + \delta h_2^2\right)^{\frac{1}{2}} \qquad \delta h_{\text{eq}} = \left(c_i^2 \delta i^2 + s_i^2 \delta\Omega^2\right)^{\frac{1}{2}} \tag{23}$$

Equation (23) shows that $\boldsymbol{\delta h}_{\text{eq}}$ has a component $hc_i \delta i$ along hs_i for constant Ω and a component $hs_i \delta\Omega$ along the orthogonal direction for constant δi. The magnitude h is taken equal to one for convenience because it is invariant for out-of-plane thrusting. This orthogonal direction is, of course, the direction along the tangent to the inclination constraint circle of radius s_i. For small inclinations, $\boldsymbol{h}$ is essentially along the pole or the inertial $\hat{z}$ direction, and the projection of the circular edge of the spherical shell is essentially a circle. When i approaches 90 deg, this projection becomes an elongated ellipse and in the limit a straight line, as s_i tends to unity. However, the same δi rotation will be achieved regardless of the value of i because the size of $\boldsymbol{\delta i}$ or $\boldsymbol{\delta h}$ is independent of i, but its projection in the h_1, h_2 plane is $\delta i c_i$, which tends to zero reducing the semiminor axis of the projected ellipse to zero, too. For example, $\delta i = i_1 - i_j = 0.0408107$ deg and $\delta\Omega = -0.528332$ deg correspond to $\delta h_{\text{eq}} = 7.124629 \times 10^{-4}$ from Eq. (20), which is close to $\Delta h_{\text{eq}} = 7.123891 \times 10^{-4}$ obtained earlier. These two numbers are also comparable to the relative inclination change $\Delta i = 0.040817$ deg obtained earlier. In fact, Δi is essentially equal to Δh_{eq}, and the small difference with δh_{eq} is due to the truncation of the higher-order terms in computing δh_1 and δh_2 and, therefore, of δh_{eq}. It is, perhaps, better to compute Δh_{eq} for a more precise evaluation of the change in the distance between two (h_1, h_2) pairs or equivalently two (i, Ω) pairs.

V. Optimal i, Ω Steering

This section develops an optimal maneuvering strategy that factors the natural drift of the spacecraft orbit between two successive thrusting cycles. Instead of targeting to the final conditions (i_2, Ω_2) as in the preceding section, intermediate target parameters for each thrusting cycle are generated resulting in the overall minimum accumulated thrust arcs. For the same wait period between two thrust arcs as in the suboptimal strategy, this solution will, indeed, provide the minimum-time transfer, which is also fuel-minimizing for this particular transfer with imposed target parameters.

Let us now represent this δh_{eq} by a velocity V, called the maneuvering velocity, as in Fig. 6. The natural drift, being in an anticlockwise direction, is represented by concentric circles centered at the equilibrium point $(0, h_{2e})$ with linear velocity W, called the precession velocity, and whose components along the h_1, h_2 axes are given by u and v, respectively. The problem is to return from any given (h_1, h_2) pair to any desired (h_1, h_2) target, and for our example at hand, to the ideal i_0, Ω_0 initial conditions, in minimum time such that a period of free drift takes place without any maneuvering required. This problem is now cast as a navigation problem that consists of finding the steering angle χ time history that leads to reaching the i_0, Ω_0 point in minimum time thereby using the minimum amount of fuel. This problem is identical to the Zermelo problem of navigating a ship in strong currents.[8] Given the ship's constant velocity V and heading angle χ, and given the current's u and v velocity components along general rectangular coordinates x and y, which in our case are the h_1 and h_2 coordinates, we have, from Ref. 8,

$$\dot{x} = Vc_\chi + u \tag{24}$$

$$\dot{y} = Vs_\chi + v \tag{25}$$

with Hamiltonian

$$H = 1 + \lambda_x(Vc_\chi + u) + \lambda_y(Vs_\chi + v) \tag{26}$$

for a minimum-time solution. The Euler–Lagrange and optimality conditions can be written as

$$\dot{\lambda}_x = \frac{-\partial H}{\partial x} = -\lambda_x \frac{\partial u}{\partial x} - \lambda_y \frac{\partial v}{\partial x} \tag{27}$$

$$\dot{\lambda}_y = \frac{-\partial H}{\partial y} = -\lambda_x \frac{\partial u}{\partial y} - \lambda_y \frac{\partial v}{\partial y} \tag{28}$$

$$\frac{\partial H}{\partial \chi} = 0 = V(-\lambda_x s_\chi + \lambda_y c_\chi) \tag{29}$$

Equation (29) yields the optimal steering angle χ with $\tan\chi = \lambda_y/\lambda_x$, and because we are minimizing transit time, the transversality condition is given by $H_f = 0$. The system is autonomous so that H is constant and, therefore, equal to zero throughout. If we replace $\lambda_y = \lambda_x \tan\chi$ in $H = 0$ of Eq. (26), then

$$\lambda_x = \frac{-c_\chi}{V + uc_\chi + vs_\chi} \tag{30}$$

$$\lambda_y = \frac{-s_\chi}{V + uc_\chi + vs_\chi} \tag{31}$$

Replacing these two adjoints in Eq. (27) with

$$\dot{\lambda}_x = \frac{s_\chi(V + uc_\chi + vs_\chi)\dot{\chi} + c_\chi(vc_\chi - us_\chi)\dot{\chi}}{(V + uc_\chi + vs_\chi)^2}$$

results in

$$(Vs_\chi + v)\dot{\chi} = (V + uc_\chi + vs_\chi)\left(c_\chi \frac{\partial u}{\partial x} + s_\chi \frac{\partial v}{\partial x}\right) \tag{32}$$

and, similarly from Eq. (28),

$$-(Vc_\chi + u)\dot{\chi} = (V + uc_\chi + vs_\chi)\left(c_\chi \frac{\partial u}{\partial y} + s_\chi \frac{\partial v}{\partial y}\right) \tag{33}$$

If we multiply Eq. (32) by s_χ and Eq. (33) by $-c_\chi$ and add, we get

$$\dot{\chi} = s_\chi c_\chi \left[\frac{\partial u}{\partial x} - \frac{\partial v}{\partial y}\right] + s_\chi^2 \frac{\partial v}{\partial x} - c_\chi^2 \frac{\partial u}{\partial y} \tag{34}$$

The simultaneous integration of Eqs. (24), (25), and (34) will yield the desired optimal trajectory. If u and v are not constant, $\dot{\chi} \neq 0$ and, therefore, $\chi \neq$ const indicating a variable-heading strategy. From Fig. 6, we have $u = Wc_\varepsilon = \omega r c_\varepsilon$ and $v = Ws_\varepsilon = \omega r s_\varepsilon$ and $\omega = \dot{\varepsilon}$,

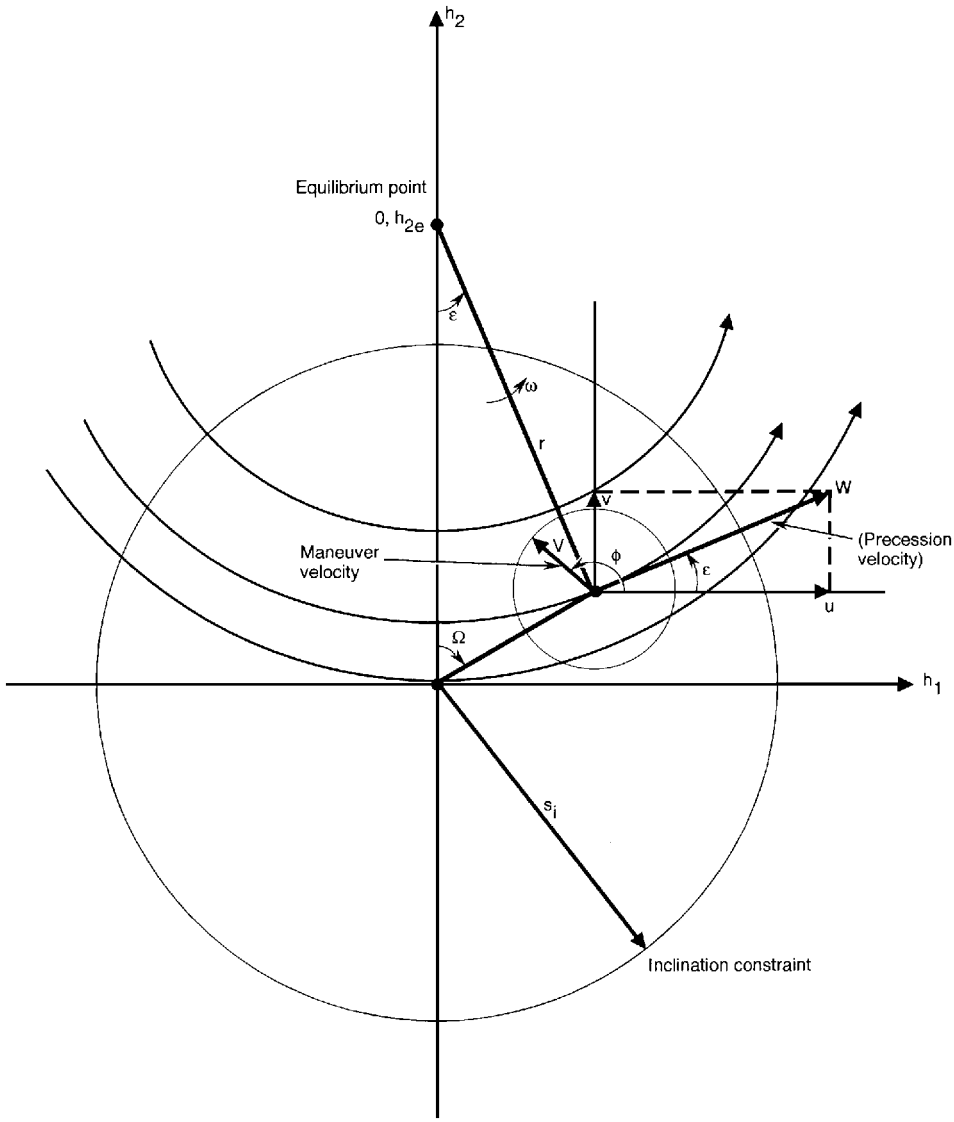

Fig. 6 Low-thrust steering geometry.

the constant angular velocity of r or the precession rate. Because $rs_\varepsilon = h_1$ and $rc_\varepsilon = h_{2e} - h_2$, we have

$$u = \omega(h_{2e} - h_2) \tag{35}$$

$$v = \omega h_1 \tag{36}$$

The dynamic equations can now be written as

$$\dot{h}_1 = Vc_\chi + \omega(h_{2e} - h_2) \tag{37}$$

$$\dot{h}_2 = Vs_\chi + \omega h_1 \tag{38}$$

with constant zero Hamiltonian

$$H = 1 + \lambda_{h_1}[Vc_\chi + \omega(h_{2e} - h_2)] + \lambda_{h_2}(Vs_\chi + \omega h_1) = 0 \tag{39}$$

The Euler–Lagrange equations for the adjoints, as well as the optimality condition, are given by

$$\dot{\lambda}_{h_1} = -\lambda_{h_2}\omega \tag{40}$$

$$\dot{\lambda}_{h_2} = \lambda_{h_1}\omega \tag{41}$$

$$\frac{\partial H}{\partial \chi} = 0 = V\left(-\lambda_{h_1}s_\chi + \lambda_{h_2}c_\chi\right) \tag{42}$$

As before, $\tan\chi = \lambda_{h_2}/\lambda_{h_1}$, and because $\partial u/\partial h_1 = 0$, $\partial v/\partial h_2 = 0$, $\partial v/\partial h_1 = \omega$, and $\partial u/\partial h_2 = -\omega$, Eq. (34) yields $\dot{\chi} = \omega = \text{const}$ such that the optimal steering law is now the simple linear law

$$\chi = \omega t + \chi_0 \tag{43}$$

From Eqs. (40) and (41), we have $\ddot{\lambda}_{h_2} = \dot{\lambda}_{h_1}\omega = -\lambda_{h_2}\omega^2$ and, therefore, λ_{h_2} is governed by $\ddot{\lambda}_{h_2} + \lambda_{h_2}\omega^2 = 0$, which is the equation of a linear oscillator with solution $\lambda_{h_2} = K_1\sin(\omega t + K_2)$, which also results from $\lambda_{h_1} = \dot{\lambda}_{h_2}/\omega$, $\lambda_{h_1} = K_1\cos(\omega t + K_2)$. Replacing in $\tan\chi = \lambda_{h_2}/\lambda_{h_1}$, we have $\chi = \omega t + K_2$. Therefore, K_2 is also the value of the control angle χ at time zero, χ_0. Let us now use the dimensionless variable $\upsilon' = \omega t$ and convert Eqs. (37) and (38) to

$$\frac{\mathrm{d}h_1}{\mathrm{d}\upsilon'} = \frac{V}{\omega}\cos(\upsilon' + \chi_0) + (h_{2e} - h_2) \tag{44}$$

$$\frac{\mathrm{d}h_2}{\mathrm{d}\upsilon'} = \frac{V}{\omega}\sin(\upsilon' + \chi_0) + h_1 \tag{45}$$

where the derivatives are now with respect to υ'. From Eqs. (44) and (45), we have

$$\frac{\mathrm{d}^2h_2}{\mathrm{d}\upsilon'^2} = \frac{V}{\omega}\cos(\upsilon' + \chi_0) + \frac{\mathrm{d}h_1}{\mathrm{d}\upsilon'} = \frac{2V}{\omega}\cos(\upsilon' + \chi_0) + (h_{2e} - h_2)$$

and, therefore, the forced oscillator type of equation

$$\frac{\mathrm{d}^2h_2}{\mathrm{d}\upsilon'^2} + h_2 = h_{2e} + \frac{2V}{\omega}\cos(\upsilon' + \chi_0) \tag{46}$$

whose solution is given by

$$h_2 = C_1 \sin(\upsilon' + C_2) + \int_0^{\upsilon'} h_{2e} \sin(\upsilon' - s)\, \mathrm{d}s$$

$$+ \frac{2V}{\omega} \int_0^{\upsilon'} \cos(s + \chi_0)\sin(\upsilon' - s)\, \mathrm{d}s$$

which reduces to

$$h_2 = C_1 \sin(\upsilon' + C_2) + h_{2e}(1 - c_{\upsilon'})$$

$$+ (V/\omega)\left[\upsilon' \sin(\upsilon' + \chi_0) - s_{\chi_0} s_{\upsilon'}\right] \tag{47}$$

At $\upsilon' = 0$,

$$h_2 = h_{20} = C_1 \sin C_2 \tag{48}$$

If we use the solution for h_2 in Eq. (44) and solve for h_1 in a similar manner used in solving for h_2, we get

$$h_1 = h_{10} + h_{2e} s_{\upsilon'} + C_1 \cos(\upsilon' + C_2) - (V/\omega) s_{\chi_0} c_{\upsilon'}$$

$$+ (V/\omega)\upsilon' \cos(\upsilon' + \chi_0) - C_1 \cos C_2 + (V/\omega) s_{\chi_0} \tag{49}$$

From Eqs. (45) and (47), we have

$$\frac{\mathrm{d}h_2}{\mathrm{d}\upsilon'} = \frac{V}{\omega}\sin(\upsilon' + \chi_0) + h_1 = C_1 \cos(\upsilon' + C_2) + h_{2e} s_{\upsilon'}$$

$$+ \frac{V}{\omega}\left[\sin(\upsilon' + \chi_0) + \upsilon' \cos(\upsilon' + \chi_0) - s_{\chi_0} c_{\upsilon'}\right]$$

and at $\upsilon' = 0$,

$$(V/\omega) s_{\chi_0} + h_{10} = C_1 \cos C_2 \tag{50}$$

Equations (48) and (50) yield

$$\tan C_2 = \frac{h_{20}}{(V/\omega) s_{\chi_0} + h_{10}} \tag{51}$$

and

$$C_1 = \left\{h_{20}^2 + \left[(V/\omega) s_{\chi_0} + h_{10}\right]^2\right\}^{\frac{1}{2}} \tag{52}$$

The initial angle χ_0 and final υ_f' are obtained from the boundary conditions at the final time υ_f', namely, $h_1(\upsilon_f') = h_{1f}$ and $h_2(\upsilon_f') = h_{2f}$. A few iterations are needed to solve for χ_0 and υ_f' by way of a Newton–Raphson scheme, which in turn completely define the optimal trajectory $h_1 = f(\upsilon')$, $h_2 = f(\upsilon')$ that starts from given h_{10}, h_{20} and achieves the final desired h_{1f}, h_{2f} in minimum time.

VI. Results

Let us use $\Delta h = 7.123891 \times 10^{-4}$, which corresponds to our 1-h low-thrust acceleration. If this maneuver is applied, e.g., once a week or Δt, then our velocity $V = \Delta h/\Delta t = 1.017 \times 10^{-4}$/day. The precession rate ω is obtained from $\omega = 2\pi/(54 \times 365.25) = 3.1856 \times 10^{-4}$ rad/day. For $i_{\max} = 0.3$ deg, we have $\Omega_1 = 87.701$ deg, $\Omega_2 = 272.299$ deg, $h_{10} = 0.52317 \times 10^{-2}$, $h_{20} = 0.21003 \times 10^{-3}$, $h_{1f} = -0.52317 \times 10^{-2}$, and $h_{2f} = 0.21003 \times 10^{-3}$. The solution is found with $\chi_0 = 178.414$ deg, $\upsilon_f' = 0.553569 \times 10^{-1}$ corresponding to a total time $t_f = \upsilon_f'/\omega = 173.77068$ days. The free-drift time $T_{\max} = \theta_{\max}/\omega$ with $\theta_{\max}/2 = \tan^{-1}[h_{1f}/(h_{2e} - h_{2f})] = -2.298$ deg is $T_{\max} = 251.91244$ days. Figure 7 shows both the optimal free-drift and low-thrust return trajectories with a combined cycle time of 425.68312 days. Figure 8 shows the optimal free-drift and maneuvering trajectories for a 4-deg inclination deadband. Here, $\Omega_1 = 57.695$ deg, $\Omega_2 = 302.305$ deg, $h_{10} = 0.58959 \times 10^{-1}$, $h_{20} = 0.37279 \times 10^{-1}$, $h_{1f} = -0.58959 \times 10^{-1}$, and $h_{2f} = 0.37279 \times 10^{-1}$. The solution for the linear χ steering program is given by $\chi_0 = 165.585$ deg with $\upsilon_f' = 0.503157$ corresponding to $t_f = 1579.45845$ days or 4.32432 years. The free-drift time $T_{\max} = 3539.81281$ days or 9.69147 years for a total cycle time of 5119.27126 days. Figure 8 also shows a smaller cycle consisting of returning to the zero-inclination target or the origin of the h_1, h_2 frame. The free-drift portion of this smaller cycle consists of one-half of the total arc that passes through the origin at midtime. This is the so called zero-inclination (ZI) strategy, which is not optimal since the deadband is consumed much faster than is the case with the optimal drift.[7] The total free-drift time for this suboptimal drift is obtained from $T_1 = \theta_{\mathrm{ZI}} P/(2\pi)$ with $\theta_{\mathrm{ZI}} = 4 \sin^{-1}[s_{i_0}/(2h_{2e})]$ (Ref. 7). The coordinates of the point of intersection with the constraint circle h_{10}' and h_{20}' are obtained from the simultaneous solution of the following two equations:

$$h_{10}'^2 + h_{20}'^2 = s_{i_{\max}}^2 \tag{53}$$

$$(h_{20}' - h_{2e})^2 = h_{2e}^2 - h_{10}'^2 \tag{54}$$

Equation (54) is the equation of the precession circle that passes through the origin and, therefore, has radius h_{2e}. This leads to

$$h_{10}' = \frac{s_{i_{\max}}}{2h_{2e}}\left(4h_{2e}^2 - s_{i_{\max}}^2\right)^{\frac{1}{2}} \tag{55}$$

$$h_{20}' = \frac{s_{i_{\max}}^2}{2h_{2e}} \tag{56}$$

We have $h_{10}' = 0.67219 \times 10^{-1}$, $h_{20}' = 0.18639 \times 10^{-1}$, with $\chi_0 = 185.364$ deg and $\upsilon_f' = 0.353740$ corresponding to $t_f = 1110.42294$ days. The free-drift time is given by $T_1/2 = 1698.24424$ days for a combined cycle time of 2808.66718 days. This shows that in the

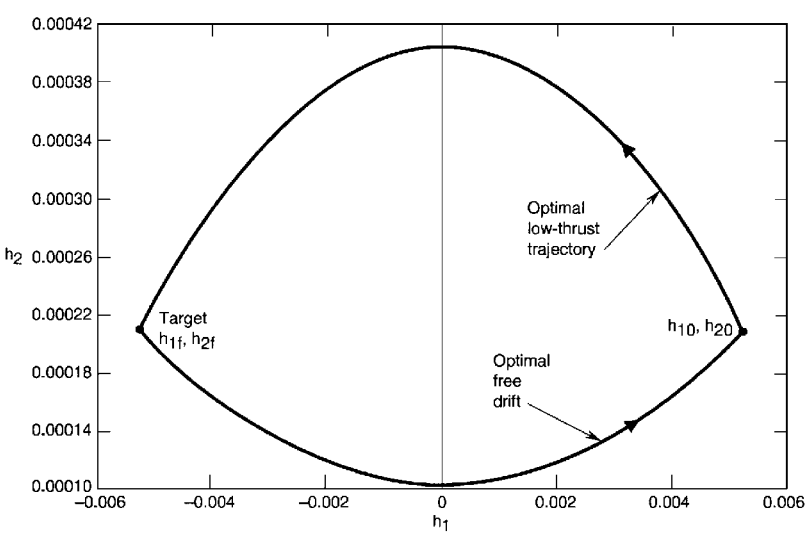

Fig. 7 Optimal low-thrust return trajectory for 0.3-deg inclination deadband.

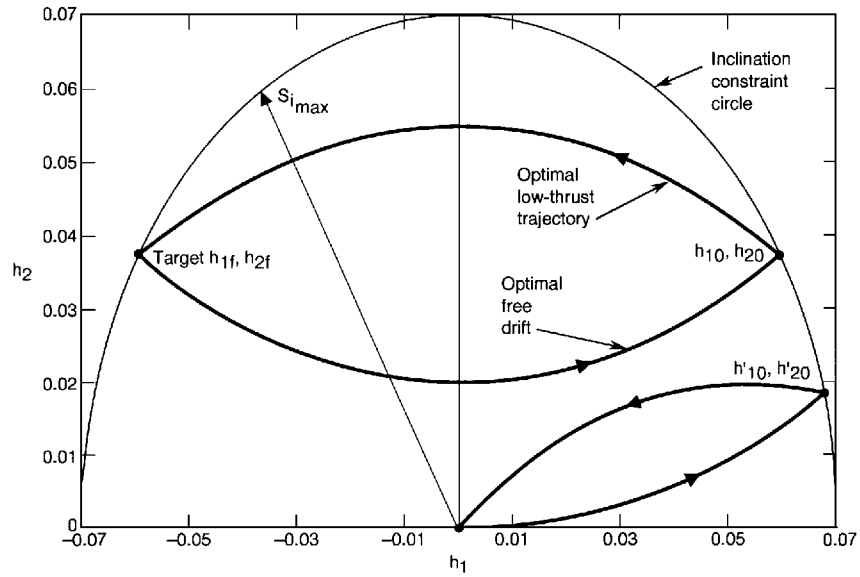

Fig. 8 Optimal low-thrust return trajectory for 4-deg inclination deadband.

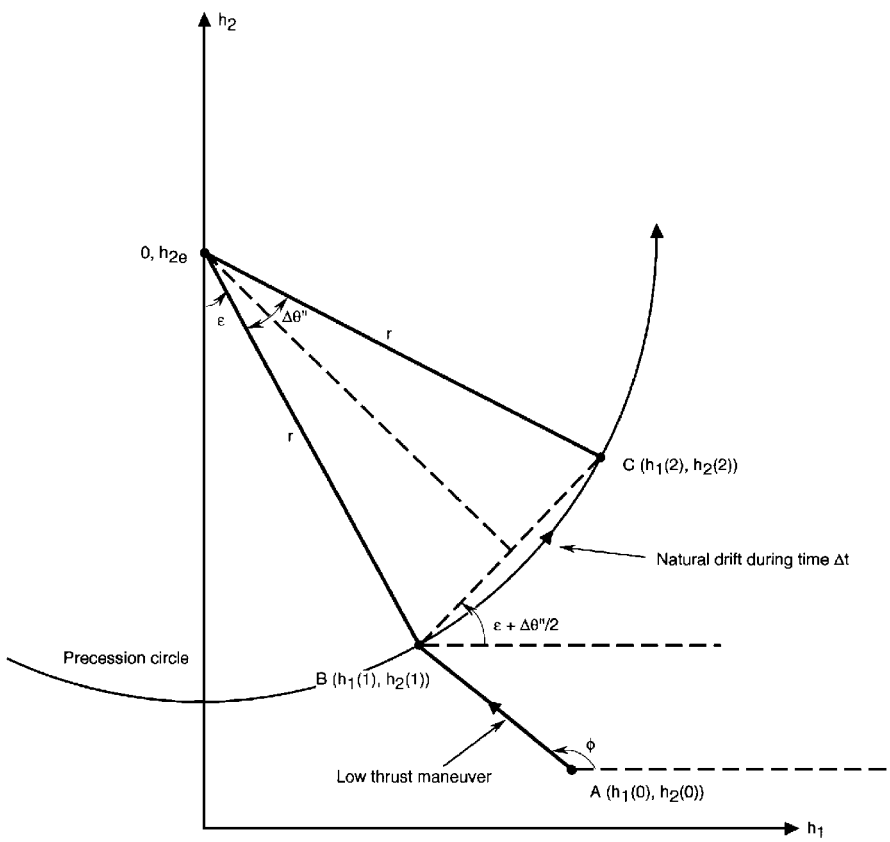

Fig. 9 Geometry of low-thrust maneuver and subsequent drift.

free-drift trip-time-maximizing optimal-cycle case the thrust period is 30.853% of the total cycle time, whereas it is at a much higher rate of 39.535% for the ZI suboptimal cycle. The optimal cycle shows similar gains over other suboptimal strategies whose target coordinates are below the optimal free-drift curve. However, these gains are important for large deadbands of the order of a few degrees such as in this example. They become vanishingly small for small tolerances, say of the order of a fraction of a degree. For example, for our $i_{\max} = 0.3$-deg case, we have for the ZI target strategy $h'_{10} = 0.52349 \times 10^{-2}$, $h'_{20} = 0.10501 \times 10^{-3}$ with $\chi_0 = 180.354$ deg and $\upsilon'_f = 0.027737$ corresponding to $t_f = 87.070701$ days. The free-drift time is given by $T_1/2 = 125.93087$ days for a combined cycle time of 213.00157 days. This shows that for the ZI case, the thrust period is 40.878% of the total cycle time, whereas it is only slightly better at 40.821% for the free-drift trip-time-maximizing cycle. If the mission lifetime is very large, so that several such cycles are required, and if the maximum free-drift time is not desired, then it is more fuel efficient to use smaller size cycles by targeting each time to a point on the constraint circle lying above the target that corresponds to the maximum free-drift time.

For our 4-deg case, let $h''_{10} = 0.3 \times 10^{-1}$, $h''_{20} = 0.629759 \times 10^{-1}$, $h''_{1f} = -0.3 \times 10^{-1}$, and $h''_{2f} = 0.629759 \times 10^{-1}$ with a free-drift period of 2623.95476 days and whose trajectory is lying above the optimal free-drift trajectory of Fig. 8. The low-thrust return from h''_{10}, h''_{20}, to h''_{1f}, h''_{2f} is given by $\chi_0 = 173.222$ deg and $\upsilon'_f = 0.236569$ corresponding to $t_f = 742.61420$ days. The thrust period for this smaller cycle is now 22.058% of the total cycle time, as opposed to the 30.853% of the long free-drift maximizing cycle

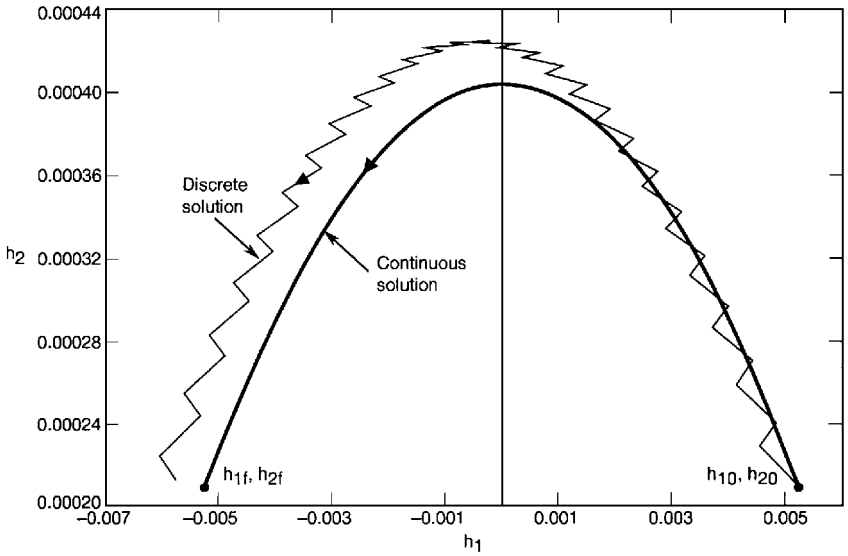

Fig. 10 Continuous and discretized optimal return trajectories for 0.3-deg inclination deadband.

of Fig. 8. This represents a relative drop of some 28%, which can be further improved for smaller cycles near the top of the constraint circle. In the limit it is most fuel efficient to remain at the top of the constraint circle and use the appropriate level of thrusting to counter the effect of the precession or, in practice, journeying through infinitesimal cycles. This is because W has the smallest value there, or in Zermelo's sense, the current is the weakest. This observation is also true for the impulsive case, which for our two $i_{\max} = 4$-deg examples, we need, respectively, $\Delta\,\Omega \simeq 115$ deg and $\Delta\,V \simeq 362$ m/s for the long cycle and $\Delta\,\Omega \simeq 51$ deg, $\Delta\,V \simeq 184$ m/s for the shorter cycle, or a drop from 1.02×10^{-1} m/s/day to 7.01×10^{-2} m/s/day with a savings of some 31%.

The fuel-minimizing solution would also consist of journeying through infinitesimal cycles near the top of the constraint circle as for the low-thrust case. If we now assume that the short thrust arcs are quasi-instantaneous compared to the period of drift between such thrust arcs, then we can discretize the continuous trajectories by using the optimal control law $\chi = \upsilon' + \chi_0$ from the continuous solution to compute the coordinates of point B given the initial conditions in point A (Fig. 9). Thus, $h_1(1) = h_1(0) + Vc_\chi$ and $h_2(1) = h_2(0) + Vs_\chi$. The jump from A to B is due to the short low-thrust arc, whereas point C is reached $\Delta\,t$ time later from B by way of the precession circle whose radius is given by $r = \{h_1^2(1) + [h_2(1) - h_{2e}]^2\}^{1/2}$. The angle ε is obtained from $\varepsilon = \tan^{-1}\{h_1(1)/[h_{2e} - h_2(1)]\}$, and the angular motion $\Delta\,\theta''$ in time $\Delta\,t$ obtained from $\Delta\,\theta'' = \omega \cdot \Delta\,t$. The segment BC has length $d = 2r\sin(\Delta\,\theta''/2)$ and, therefore, the coordinates of C are $h_1(2) = h_1(1) + \mathrm{d}\cos[\varepsilon + (\Delta\,\theta''/2)]$ and $h_2(2) = h_2(1) + \mathrm{d}\sin[\varepsilon + (\Delta\,\theta''/2)]$. These steps are repeated for the next thrust arc and drift period until the final time υ'_f is reached.

Figure 10 shows both the continuous optimal trajectory as well as the discretized equivalent trajectory with a good match for the case of the 0.3-deg inclination tolerance. In this case, a final trim is needed to match exactly the final conditions h_{1f} and h_{2f}, and this can be accomplished by adjusting the angular position of the final thrust arc along the spacecraft orbit and using a longer thrust arc to reach the target if necessary.

VII. Conclusions

An optimal steering strategy for the north–south stationkeeping of geostationary spacecraft using infrequent low-thrust maneuvers has been devised. The optimal drift cycle in inclination and node depicted by Kamel and Tibbitts' zeroth-order analytic solution is adopted as an example, as the ideal drift cycle to repeat, once the inclination tolerance deadband is violated. The recovery of the ideal initial conditions or any other desired target conditions, achieved by a single impulse with chemical thrusters requires a series of short-duration low-thrust arcs judiciously positioned along the current spacecraft orbit such that these conditions are reached in minimum time and, therefore, requiring minimum propellant usage for a given common wait period between successive thrust arcs. This optimal transfer design takes into account the natural drift of the orbit plane orientation parameters during the nonmaneuvering coast arcs, by creating intermediate target conditions to be achieved by each thrust arc. This problem has been shown to be an optimal control problem of the Zermelo type for navigation in the i, Ω space. Further improvements to this analysis are possible by considering the exact numerical description of the free-drift dynamics, as well as the consideration of variable-length thrust arcs within prescribed bounds, which would be also optimized but still restricted to pure out-of-plane acceleration.

Acknowledgment

This work was supported by the U.S. Air Force Space and Missile Systems Center under Contract F04701-88-C-0089.

References

[1] Frick, R. H., and Garber, T. B., "Perturbations of a Synchronous Satellite," Rept. R-399-NASA, Rand Corp., May 1962.

[2] Allen, R. R., and Cook, G. E., "The Long-Period Motion of the Plane of a Distant Circular Orbit," *Proceedings of the Royal Society*, Vol. 280, 1964, pp. 97–109.

[3] Billik, B. H., "Cross-Track Sustaining Requirements for a 24-hr Satellite," *Journal of Spacecraft and Rockets*, Vol. 4, No. 3, 1967, pp. 297–301.

[4] Balsam, R. E., "A Simplified Approach for Correction of Perturbations on a Stationary Orbit," *Journal of Spacecraft and Rockets*, Vol. 6, No. 7, 1969, pp. 805–811.

[5] Eckstein, M. C., and Hechler, F., "Optimal Autonomous Stationkeeping of Geostationary Satellites," AAS/AIAA Astrodynamics Specialist Conf., AAS Paper 81-206, Lake Tahoe, NV, Aug. 1981.

[6] Slavinskas, D. D., Johnson, G. K., and Benden, W. J., "Efficient Inclination Control for Geostationary Satellites," AIAA Paper 85-0216, Jan. 1985.

[7] Kamel, A., and Tibbitts, R., "Some Useful Results on Initial Node Locations for Near-Equatorial Circular Satellite Orbits," *Celestial Mechanics*, Vol. 8, 1973, pp. 45–73.

[8] Bryson, A. E., and Ho, Y.-C., *Applied Optimal Control*, Ginn and Co., Waltham, MA, 1969, pp. 77–81.